https://doi.org/10.1029/2018GL078536

Interannual Variability of the Australian Summer Monsoon System Internally Sustained through Wind-Evaporation Feedback

S. Sekizawa[1], H. Nakamura[1], and Y. Kosaka[1]

[1] Research Center for Advanced Science and Technology, The University of Tokyo, Tokyo, Japan

Key Points

- Interannual convection variability in summer northern Australia is unforced by tropical ocean variability but forms a distinct variance peak
- This internal variability of the Australian summer monsoon is maintained through a wind-evaporation feedback over surrounding oceans
- Sea surface temperature anomalies act to damp the convection anomalies, but dynamical air-sea interaction weakens this damping effect

Abstract

Interannual variability of Australian summer monsoon (AUSM) activity is hardly forced locally or remotely by tropical sea surface temperature (SST) variability. Despite this lack of SST forcing, convection variability in northern Australia is so strong that it emerges as a distinct peak in climatological variance of convection in austral summer. The present study shows that an internal variability unforced by tropical SST anomaly is dominant in seasonal mean strength of the AUSM system. A mechanism that sustains convection anomaly without SST forcing is also examined. Analysis of latent heat flux reveals that under the climatological monsoon westerlies, the wind-evaporation feedback in the tropical southeastern Indian Ocean sustains anomalous convection despite a counteracting effect of SST anomalies. The wind anomalies induced by the anomalous AUSM change the subsurface southeastern Indian Ocean, which can contribute to the maintenance of the anomalous convection through weakening the damping effect by SST anomalies.

Plain Language Summary

Over most of the tropical oceans, deviations of sea surface temperature from its mean seasonal cycle drive anomalous states of atmospheric convection and rainfall. Due to slow nature of ocean variations, this relationship provides an important origin of weather predictions beyond a few weeks. However, this relationship does not always hold depending on regions and seasons. We find that year-to-year variation of the Australian summer monsoon is the most pronounced of those unforced by tropical ocean variability in austral summer. We also investigate why the summertime mean anomalous strength of the monsoon can be sustained without ocean forcing. Instead of ocean forcing, an anomalous state of the Australian summer monsoon is sustained through a positive feedback between anomalous surface wind and evaporation over the tropical southeastern Indian Ocean. Besides changes in ocean downwelling in response to the surface wind anomalies suppress sea surface temperature changes, which would otherwise spoil the wind-evaporation feedback.

1. Introduction

Many studies have investigated relationship between tropical rainfall and sea surface temperature (SST) variability, since the latter provides predictability for anomalous rainfall (e.g., Trenberth & Shea, 2005; Kumar et al., 2013). Wu and Kirtman (2007) examined local interannual correlations of rainfall with SST and its tendency, to identify multiple regimes of local air-sea interaction in the tropics based on relative importance between SST forcing and atmospheric forcing. They found that the tropical southeastern Indian Ocean (SEIO) features marked seasonality in this relative importance. In winter to spring, rainfall is positively correlated with underlying SST, indicating dominance of SST forcing to local rainfall. In contrast, it is negatively correlated with both SST and its tendency during summer, indicating dominant atmospheric forcing to the ocean.

Hendon et al. (2012) highlighted lower seasonal predictability of precipitation around northern Australia (NAUS) during the Australian summer monsoon (AUSM) than in the premonsoon season. They attributed this predictability decrease to the climatological reversal of surface easterlies to westerlies over the tropical SEIO including the Timor Sea (Figures 1a and b), which is vital for the wind-evaporation-SST (WES) feedback (Xie & Philander 1994). Namely, the prevailing AUSM westerlies preclude the WES feedback, and therefore SST anomalies in the adjacent seas can no longer support anomalous monsoonal rainfall.

Despite the lack of the WES feedback, interannual rainfall variability is still pronounced around NAUS in summer. Indeed, interannual variance of convection activity has a well-defined maximum over NAUS (Figure 1c). In sharp contrast to the variability maxima around the Philippines and equatorial Pacific, the convection variability over NAUS is in large part unforced by tropical seasonal-mean SST variability (Figures 1d and e), which is consistent with Hendon et al. (2012). This study is the first to demonstrate that the pronounced variability in convective rainfall over NAUS is a manifestation of self-sustained internal variability of the AUSM system. Anomalous seasonal mean strength of the AUSM requires some maintenance mechanisms rather than large-scale SST anomaly. Thus, we investigate its possible maintenance mechanisms in terms of moisture supply and air-sea interaction over the tropical SEIO.

2. Data

To examine AUSM variability, we use rain-gauge observations at seven stations in NAUS, as indicated in the right panel of Figure 2a, obtained from the Australian Bureau of Meteorology. Our analysis also uses outgoing longwave radiation (OLR) from the National Oceanic and Atmospheric Administration (NOAA) at 2.5º resolution (Liebmann and Smith 1996), gridded precipitation data set of the Climate Prediction Center Merged Analysis of Precipitation based on satellite estimates and gauge data with 2.5º resolution (Xie & Arkin 1997), SST from the Hadley Centre Sea Ice and SST with 1º resolution (Rayner et al. 2003), and the Japanese 55-year reanalysis (JRA-55) of the global atmosphere with 1.25º resolution (Kobayashi et al. 2015). Relationship of the AUSM variability with the Madden-Julian Oscillation (MJO) is examined with daily OLR-based MJO index (OMI) from the NOAA Earth System Research Laboratory (Kiladis et al. 2014). We define eight MJO phases in the phase space spanned by OMI2 and –OMI1, in accordance with the conventional phase diagram by Wheeler and Hendon

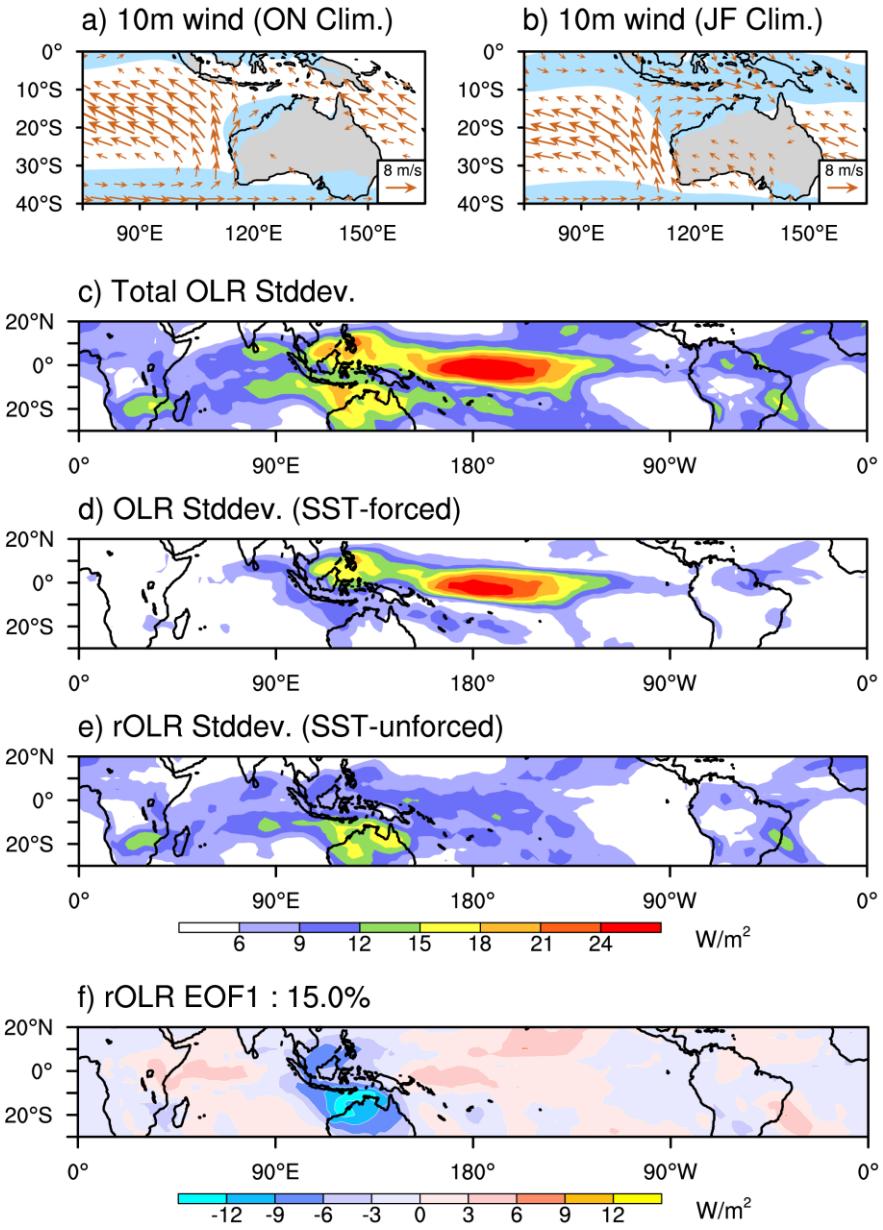

Figure 1. (a) ON and (b) JF climatologies of 10-m wind. Scaling of the vectors is given at the right bottom of each panel. Blue shadings indicate the region of westerly zonal wind. Climatological standard deviation of (c) total, (d) SST-forced and (e) SST-unforced components of JF-mean OLR. (f) EOF1 of the SST-unforced variability of JF mean OLR (rOLR). Details of the analysis method for (c)–(f) are described in Text S1.

(2004). When OMI amplitude is less than a unit standard deviation, we regard that the MJO is weak irrespective of its phase.

We further investigate the impacts of the AUSM variability on interior of the SEIO, using monthly mean water temperature data of the Ocean Reanalysis System 4 from the European Centre for Medium-Range Weather Forecasts (ECMWF) with horizontal resolution of 1° and 42

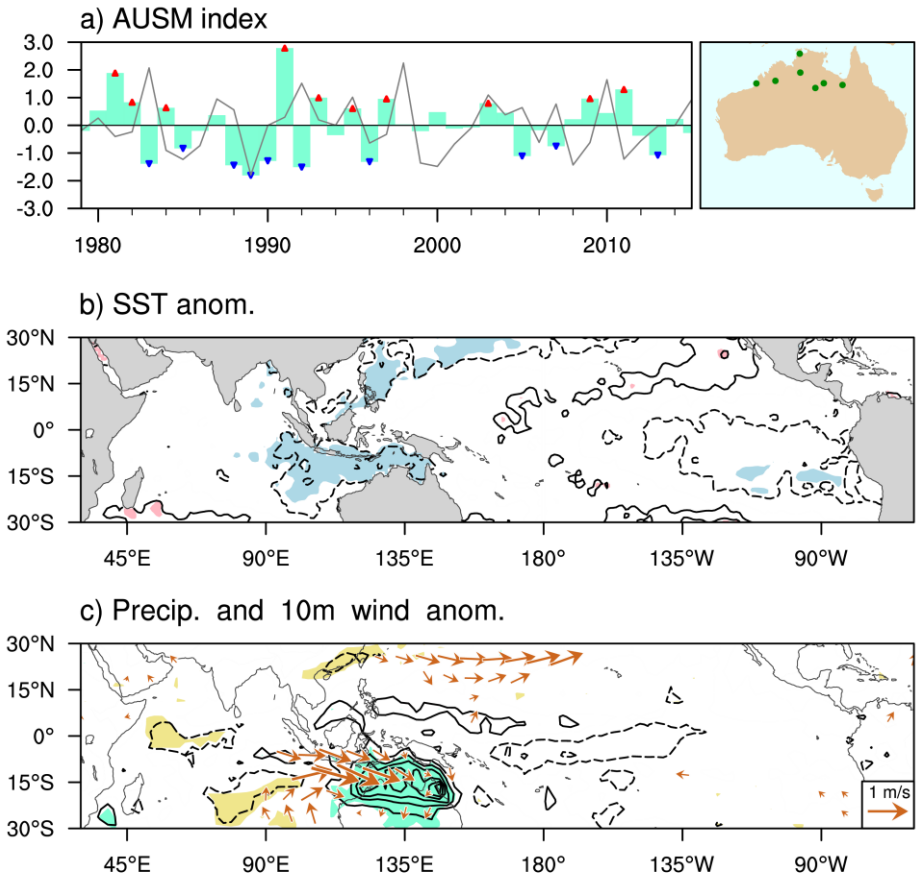

Figure 2. (a) Standardized time series of the AUSM index (green bar) and JF Niño 3.4 SST (gray line). Red and blue triangles denote 10 summers of the most strong and weak AUSM, respectively, used for composite analyses. Locations of seven stations for deriving the AUSM index are indicated in the right panel. JF anomalies in (b) SST and (c) precipitation regressed onto the AUSM index with contour intervals of 0.1 ºC and 0.5 mm/day, respectively. Solid and dashed contours indicate positive and negative anomalies, respectively. Zero contours are omitted. Color shading represents the 95% confidence level. In (c), vectors show the corresponding 10-m wind anomalies (plotted only where either of their zonal and meridional component is statistically confident at the 95% level). Scaling of the vectors is given at the right bottom of the panel.

vertical levels at 10- to 15-m thickness in the upper 200 m (Balmaseda et al. 2013). Following Du et al. (2005), we define the mixed layer bottom at which temperature is 0.8 ^{o}C below SST.

As the summer monsoon season begins between mid-December and mid-January and terminates around March (Holland 1986; Drosdowsky 1996; Kajikawa et al. 2010), we focus on January–February (JF) season. The analysis period is from 1979 to 2015 except for OLR, which is available only until 2012. We have linearly detrended each variable before calculating anomalies. In regression and composite analyses, we test statistical significance based on the two-tailed *t* test with degrees of freedom based on number of sample years.

3. Basic Structure and Property of the AUSM

Climatological variance of tropical convection in austral summer peaks over the equatorial Pacific and extends westward, forming northern and southern lobes. In order to assess SST influence on this convection variability in the tropics, we first decompose interannual variability of JF mean OLR statistically into SST-forced and unforced components. This is achieved by regressing tropical OLR anomalies onto the five leading principal components of seasonal mean tropical SST (20ºS–20ºN), which explain 85% of total SST variance in accumulation (see supporting information Text S1 for detail). The residual, denoted as rOLR variability, is virtually uncorrelated with large-scale tropical SST variability. As shown in supporting information Figure S1, this is confirmed also with an atmospheric general circulation model experiment with Geophysical Fluid Dynamics Laboratory AM 2.1 (Anderson et al. 2005) driven by climatology of NOAA optimum interpolated SST (Reynolds et al. 2007) (see supporting information Text S2 for detail). Without contribution from the SST-unforced convection variability, the southern hemispheric lobe of the climatological convection variability would almost disappear (Figure 1d). By contrast, climatological variability maxima in the equatorial Pacific and around the Philippines (Figure 1c) are associated with El Niño–Southern Oscillation.

The leading empirical orthogonal function (EOF) mode of rOLR features a monopole structure centered at NAUS (Figure 1f), illustrating that NAUS is the center of action of the SST-unforced convection variability. This analysis is, however, subject to some arbitrariness in statistical handling (e.g., the number of EOF modes of tropical SST subtracted). To avoid this issue while exploiting higher reliability of direct precipitation measurements, we hereafter use rain-gauge observations in NAUS to represent AUSM variability. Referring to Figure 1f, we simply average JF mean precipitation across the seven stations to define an AUSM index (Figure 2a). This simple index is indeed highly correlated with the leading principal component of rOLR (r = 0.71).

Our station-based index confirms that the AUSM variability arises mostly from atmospheric internal variability. SST anomalies in JF regressed onto the AUSM index are generally weak and not well organized in the tropics (Figure 2b). A notable exception is a weak but significant SST anomaly in the tropical SEIO. However, its sign is negative despite locally enhanced convection, indicating dominance of atmospheric forcing to the ocean. Westerly wind anomalies induced by enhanced convection (Figure 2c) strengthen climatological monsoonal westerlies (Figure 1b), to cool underlying SST as discussed below. These features of anomalies are nearly identical to those demonstrated by Hendon et al. (2012). Furthermore, correlation between the AUSM index and Niño 3.4 SST is quite low (r = –0.07, Figure 2a), and there is virtually no signal of tropical SST anomalies in the preceding austral spring (not shown). These results substantiate that the variability of the AUSM is unlikely forced either locally or remotely by tropical SST variability, consistent with Hendon et al. (2012). Figure 2c also illustrates localized structure of the AUSM variability with significant positive anomalies of precipitation confined to NAUS, as extracted in the leading EOF of rOLR (Figure 1f). As shown in Fig. 2c, the corresponding surface wind anomalies are also confined around NAUS, forming an anomalous cyclone superposed on the climatological monsoonal circulation (Figure 1b).

The rainfall variability of our interest arises from interannual fluctuations in seasonal-mean activity of the AUSM, although intraseasonal oscillation dominates in summertime convection over this region (Hendon & Liebmann 1990; Wheeler et al. 2009). Figure 3a shows

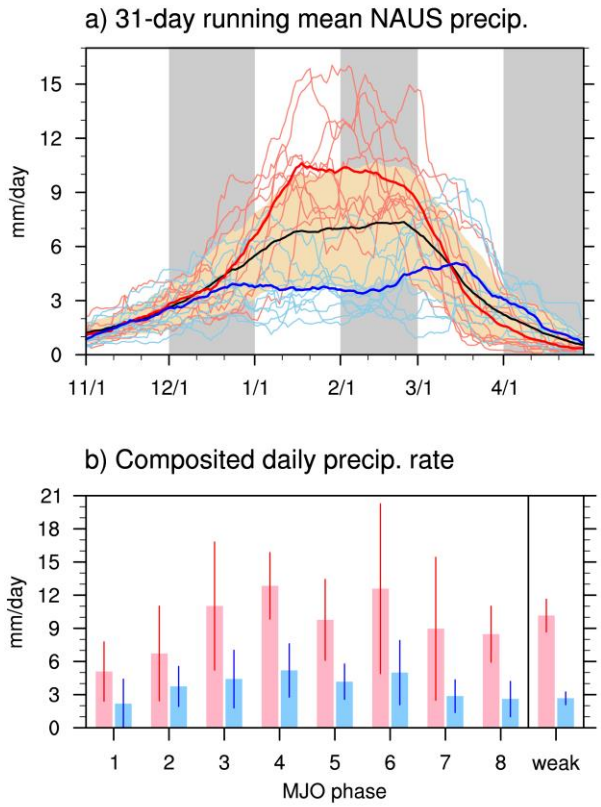

Figure 3. (a) 31-day running mean evolutions of the station-based index of NAUS precipitation for 10 strong (thin red lines) and 10 weak (thin blue lines) years of the AUSM, and the corresponding composites (thick red and blue lines for the strong and weak years, respectively). The climatological mean and standard deviation are superimposed with black line and brown shading, respectively. (b) Daily precipitation rate composited for strong (red bars) and weak (blue bars) years of the AUSM separately for individual MJO phases, with error bars indicating 95% confidence interval.

evolutions of 31-day running mean precipitation for 10 summers of the most strong and weak AUSM. The climatological seasonal cycle verifies our definition of the summer monsoon season as January and February. In this season, the interannual standard deviation is nearly as large as half of the climatological mean (Figure S2). Throughout the summer monsoon season, daily precipitation tends to fluctuate around higher and lower values than climatology in the strong and weak AUSM years, respectively, featuring pronounced interannual variability as highlighted in contrasting composited evolutions between the strong and weak AUSM years. After the retreat of AUSM, composited precipitation anomalies tends to reverse their sign, which may suggests a restoration of SST forcing. We further composite daily precipitation rates separately for the strong and weak AUSM summers for individual MJO phases. Enhanced daily precipitation in strong AUSM summer is obvious regardless of the phase and intensity of MJO (Figure 3b). We have also confirmed that there is no significant difference in number of days of each MJO phase between the strong and weak AUSM summers. Thus, the JF precipitation difference between the strong and weak AUSM years arises hardly from particular extreme MJO events but rather from persistent modulations of the summer monsoon.

4. Maintenance Mechanisms for the AUSM Variability

4.1. Moisture Supply

In order to discuss possible mechanisms for the strong AUSM variability, we first examine the anomalous surface latent heat flux over the SEIO. Following Tanimoto et al. (2003), we obtain a linearized bulk formula for the anomalous flux as

$$Q' = Q - \bar{Q} = \rho LC\{U'(\bar{q}_s - \bar{q}_a) + \bar{U}q_s' - \bar{U}q_a'\}, \qquad (1)$$

where Q denotes turbulent latent heat flux and U 10-m scalar wind speed, while q_s and q_a are saturation specific humidity at SST and 2-m specific humidity, respectively. Overbars and primes denote JF climatology and anomalies, respectively. ρ, L, and C are air density, latent heat of vaporization for water and the bulk coefficient, all of which are assumed to be constant. We can derive ρLC from climatological values as $\bar{Q}/\{\bar{U}(\bar{q}_s - \bar{q}_a)\}$, so that Eq. (1) becomes

$$Q' = \bar{Q}\frac{U'}{\bar{U}} + \bar{Q}\frac{q_s'(T_s')}{\bar{q}_s(\bar{T}_s) - \bar{q}_a} - \bar{Q}\frac{q_a'}{\bar{q}_s(\bar{T}_s) - \bar{q}_a}. \qquad (2)$$

Three terms in the right-hand side represent contributions to the anomalous flux from individual anomalies of wind speed, SST (T_s), and humidity, noting that q_s' is expressed in terms of T_s' via the Clausius-Clapeyron equation. We have confirmed that contributions from nonlinearity in JF mean anomalies and the covariance of submonthly fluctuations are both negligible. In this analysis, we use JRA-55 in locally evaluating all the variables in Eq. (2).

Figure 4a shows surface latent heat flux anomalies for the strong AUSM. Increased latent heat flux in the SEIO coincides with enhanced wind speed due to the anomalous westerlies as augmented AUSM inflow (Figures 1b and 2c). In fact, our local decomposition of the anomalous latent heat flux based on Eq. (2) reveals a significant positive contribution from the wind speed increase (Figure 4b). However, this enhanced heat flux cools the underlying ocean (Figure 2b), acting to reduce surface evaporation. This counteracting process, expressed in the SST term of Eq. (2), indeed acts to suppress the latent heat flux anomalies over the SEIO (Figure 4c). However, its magnitude is less than half of the contribution from the wind speed term (Figure 4b). In net, the anomalous surface westerlies forced by enhanced convection over NAUS can thus sustain anomalous moisture supply from the SEIO despite the slight lowering in SST.

Climatologically, the monsoonal circulation transports moisture from the SEIO into NAUS to sustain rainfall. The increased evaporation over the SEIO therefore reinforces this moisture supply to enhanced AUSM rainfall. This wind-evaporation feedback owes its effectiveness to the climatological westerlies associated with the AUSM system, prevailing only in the summer monsoon season (Figure 1b). Besides, the anomalous monsoonal inflow as a response to anomalous convection (Figure 2c) modifies intrusion of marine humid air into NAUS (vectors in Figure 4a), which is crucial for sustaining the anomalous monsoonal rainfall.

4.2. Dynamical Air-Sea Interaction

Influence of the AUSM variability extends into subsurface layers of the SEIO. In summertime climatology under the prevailing monsoonal westerlies, the oceanic mixed layer and thermocline both deepen along the southern coast of Indonesia (Figure 5b) compared to other seasons (October–November climatology is shown in Figure 5a as an example). As depicted in

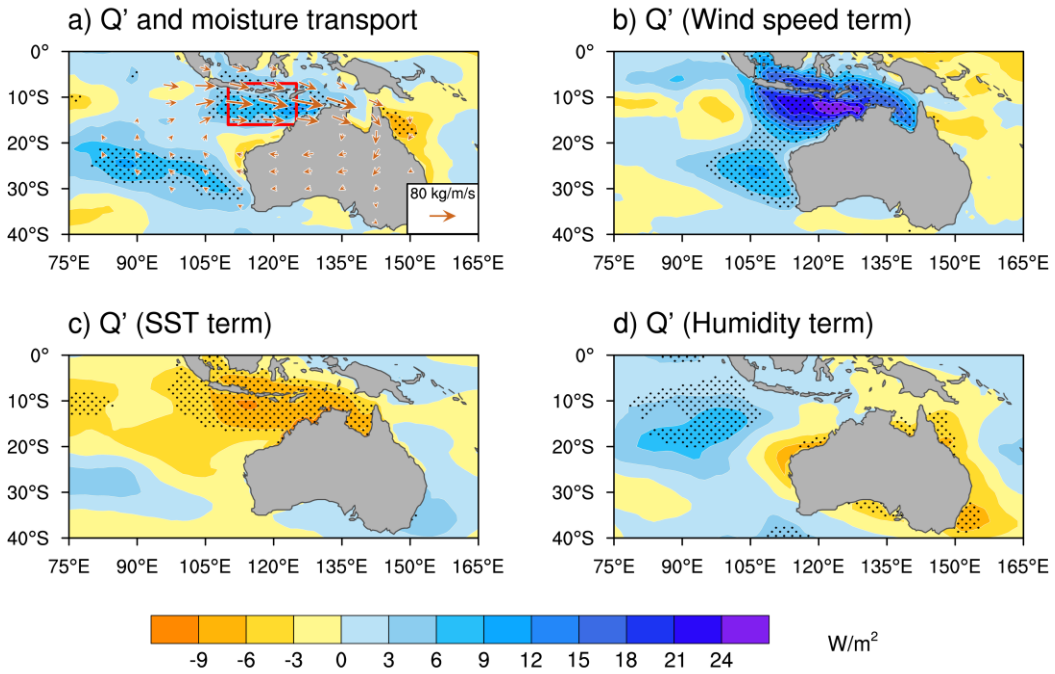

Figure 4. (a) JF surface latent heat flux anomalies regressed onto the AUSM index, representing a typical situation of the strong AUSM. (b–d) Same as in (a), but for individual contributions from anomalies in (b) wind speed, (c) SST and (d) specific humidity based on Eq. (2). Stippling represents the 95% confidence level. In (a), column integrated moisture flux anomalies are superimposed with vectors (plotted only if either of the zonal and meridional component is statistically confident at 95%), whose scaling is given at the right bottom. Red box in (a) indicates the domain for meridional cross-section in Figure 5.

Figure 5c, the anomalously strong AUSM emphasizes these climatological features. The stronger surface westerlies due to the enhanced AUSM act to cool and thicken the ocean mixed layer through augmented evaporation and mixing but at the same time lead to thermocline deepening through intensified coastal downwelling. The thermocline deepening manifests itself as warm anomalies below the mixed layer (Figure 5c).

It is noteworthy that these subsurface anomalies can suppress the negative feedback onto the anomalous NAUS convection by SST cooling. Under the strong AUSM, intensified surface westerlies lead to warmer subsurface water entrained into the climatologically deepened mixed layer. The resultant anomalous warming due to the reduced entrainment cooling acts to offset the anomalous surface evaporative cooling and thereby weaken the damping effect of the SST anomalies on anomalous convection over NAUS. Still, a quantitative analysis is needed to verify how effectively this oceanic mechanism is operative.

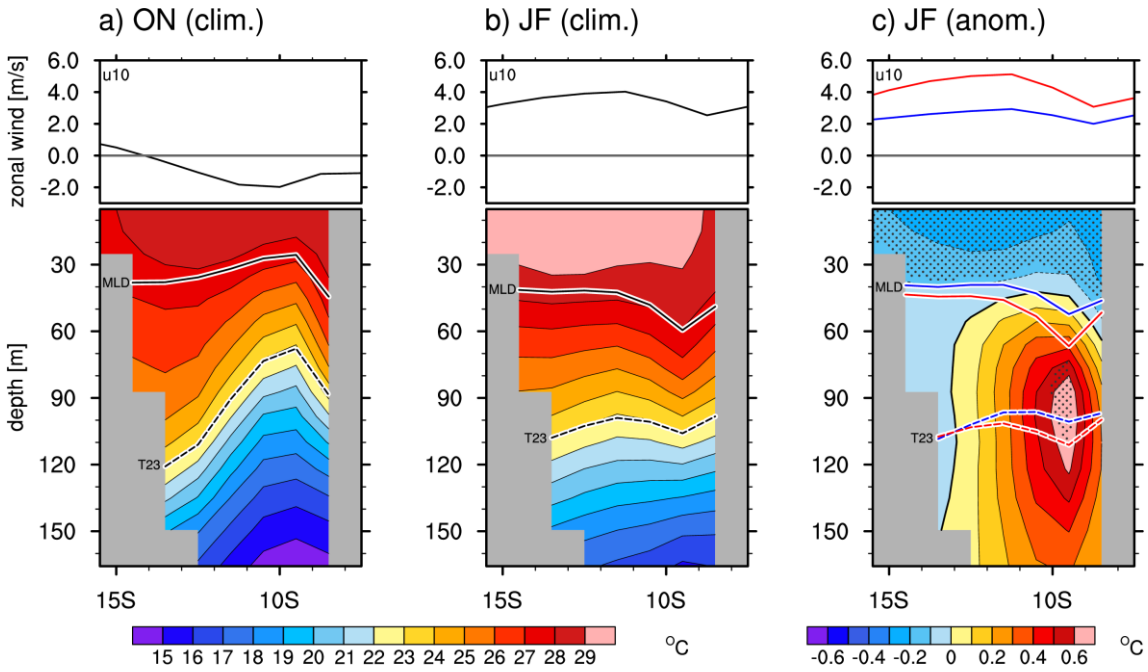

Figure 5. Meridional cross sections of longitudinal mean (110–125ºE) water temperature (shading). (a) ON climatology, (b) JF climatology, and (c) JF anomalies regressed onto the AUSM index. Stippling in (c) represents the confidence level of 95%. Black lines in (a) and (b) indicate ON and JF climatological 10-m zonal wind (top panels), mixed layer bottom (bottom panels, solid) and 23ºC isotherm (bottom panels, dashed), respectively. Red and blue lines in (c) represent their JF anomalies added onto and subtracted from the corresponding climatologies, respectively.

5. Summary and Discussion

By defining an AUSM index based on precipitation measurements in NAUS, we examined interannual variability of JF mean AUSM strength. Consistent with previous studies, the monsoon variability is unlikely forced locally or remotely by tropical SST variability (Figure 2b). Our statistical decomposition of convective anomalies into SST-forced and unforced components has revealed that NAUS is the region of the strongest SST-unforced convection variability and corresponds to a well-defined climatological maximum of convection variability. Anomalous precipitation and circulation are both confined mostly into the climatological AUSM system (Figure 2c), suggesting that the modulation of AUSM strength is internal to the monsoon system. Our analysis has also revealed that JF mean precipitation anomalies are not a reflection of extreme MJO events but due to persistent anomalous strength of the AUSM throughout the summer monsoon season (Figure 3). Surface wind anomalies over the tropical SEIO are a key factor for prominent convection anomalies in NAUS. The strong AUSM induces anomalous westerlies over the SEIO, which intensifies the climatological monsoonal circulation and thereby surface evaporation and moisture transport into NAUS (Figure 4). In addition, the AUSM variability influences subsurface temperature in the SEIO along the southern coast of Indonesia. We propose a possibility that the subsurface temperature anomalies dilute SST changes through

modulating the entrainment at the mixed layer bottom, which tends to maintain the anomalous convection over NAUS. This process may contribute to distinct decrease in persistence of SST anomalies along the coast after the AUSM onset (Figure S3).

In transition season when easterly winds dominate over the SEIO (Figure 1a), the positive WES feedback supports persistent anomalous convection, as argued by Hendon et al. (2012). They also argued that, after the AUSM onset, westerly anomalies due to enhanced convection superposed onto the climatological monsoon westerlies (Figure 1b) act to cool SST, as a negative SST-convection feedback that can demote seasonal predictability for summertime rainfall over NAUS. In this study, we rather emphasize the positive feedback, where the intensified surface westerlies enhance surface evaporation and thereby support anomalous convection even under slightly lowered SST. Because it is not until the AUSM onset that this positive feedback becomes effective, internal variability dominates in NAUS rainfall especially in the summer monsoon season. The AUSM variability, which is unforced by tropical SST anomalies but supported by wind-evaporation feedback, acts as a noise for seasonal prediction of rainfall over NAUS in summer.

The feedback effect proposed in this study should be quantitatively evaluated. Moreover, what can be a trigger of the AUSM variability is still unclear. Self-sustained feature of the AUSM variability implies that it can be triggered by various phenomena affecting this region and that it is difficult to predict it in advance. Nevertheless, there may be a possibility that anomalous AUSM activity tends to persist once initiated right after the onset, which may positively contribute to intraseasonal predictability of the AUSM.

The interannual variability of the AUSM not only affects local weather but also impacts remote climate via atmospheric teleconnections. As shown in supporting information Figure S4, we find distinct meridional wave-like pattern and wave-activity flux (Takaya & Nakamura 2001) originating from the Maritime Continent into the Far East associated with the AUSM variability. Having projection onto the Western Pacific teleconnection pattern (Wallace & Gutzler 1981), this cross-equatorial teleconnection pattern features a significant cyclonic anomaly over the midlatitude North Pacific, modulating the East Asian winter monsoon (Takaya & Nakamura 2005). Although clarification of causality requires further investigation, the AUSM variability potentially has significant impacts on East Asian wintertime climate, limiting its seasonal predictability.

Acknowledgments

We would like to thank two anonymous reviewers for their constructive comments. This study is supported in part by the Japanese Ministry of Education, Culture, Sports, Science and Technology (MEXT) through the Arctic Challenge for Sustainability (ArCS) Program and by the Japanese Ministry of Environment through the Environment Research and Technology Department Fund 2-1503. This work was also supported by the Japan Society for the Promotion of Science (JSPS) through KAKENHI Grants 15H05466 and 18H01278 and by the Japan Science and Technology Agency through Belmont Forum CRA *InterDec*. The JRA-55 reanalysis data sets are provided by Japan Meteorological Agency (JMA). HadISST data are provided by Met Office Hadley Centre from their website at http://www.metoffice.gov.uk/hadobs/hadisst/. CMAP precipitation data, interpolated OLR data and OMI index are provided by the NOAA/OAR/ESRL PSD, Boulder, Colorado, USA, from their website at http://www.esrl.noaa.gov/psd/. The ORA-S4 reanalysis data sets are provided by the Integrated Climate Data Center, Universität Hamburg, from their website at http://icdc.cen.uni-

hamburg.de/1/projekte/easy-init/easy-init-ocean.html. Rain-gauge data in Northern Australia are obtained from the website of the Australian Bureau of Meteorology at http://www.bom.gov.au/climate/data/.

References

Anderson, J. L., Balaji, V., Broccoli, A. J., Cooke, W. F., Delworth, T. L., Dixon, K. W., et al. (2005). The new GFDL global atmosphere and land model AM2–LM2: Evaluation with prescribed SST simulations. *Journal of Climate*, 17, 4641–4673, https://doi.org/10.1175/JCLI-3223.1

Balmaseda, M. A., Mogensen, K. & Weaver, A. T. (2013). Evaluation of the ECMWF ocean reanalysis system ORAS4. *Quarterly Journal of the Royal Meteorological Society*, 139, 1132–1161. https://doi.org/10.1002/qj.2063

Drosdowsky, W. (1996). Variability of the Australian summer monsoon at Darwin. 1957–1992. *Journal of Climate*, 9, 85–96. https://doi.org/10.1175/1520-0442(1996)009<0085:VOTASM>2.0.CO;2

Du, Y., Qu, T., Meyers, G., Masumoto, Y., & Sasaki, H. (2005). Seasonal heat budget in the mixed layer of the southeastern tropical Indian Ocean in a high-resolution ocean general circulation model. *Journal of Geophysical Research*, 110, C04012. https://doi.org/10.1029/2004JC002845

Hendon, H. H., & Liebmann, B. (1990). The intraseasonal (30–50 day) oscillation of the Australian summer monsoon. *Journal of the Atmospheric Sciences*, 47, 2909–2924. https://doi.org/10.1175/1520-0469(1990)047<2909:TIDOOT>2.0.CO;2

Hendon, H. H., Lim, E.-P., & Liu, G. (2012). The role of air-sea interaction for prediction of Australian summer monsoon rainfall. *Journal of Climate*, 25, 1278–1290. https://doi.org/10.1175/JCLI-D-11-00125.1

Holland, G. J. (1986). Interannual variability of the Australian summer monsoon at Darwin: 1952–82. *Monthly Weather Review*, 114, 594–604. https://doi.org/10.1175/1520-0493(1986)114<0594:IVOTAS>2.0.CO;2

Kajikawa, Y., Wang, B., & Yang, J. (2010). A multi-time scale Australian monsoon index. *International Journal of Climatology*, 30, 1114–1120. https://doi.org/10.1002/joc.1955

Kiladis, G. N., Dias, J., Straub, K. H., Wheeler, M. C., Tulich, S. N., Kikuchi, K., et al. (2014). A Comparison of OLR and Circulation-Based Indices for Tracking the MJO. *Monthly Weather Review*, 142, 1697–1715. https://doi.org/10.1175/MWR-D-13-00301.1

Kobayashi, S., Ota, Y., Harada, Y., Ebita, A., Moriya, M., Onoda, H., et al. (2015). The JRA-55 reanalysis: General specifications and basic characteristics. *Journal of the Meteorological Society of Japan*, 93, 5–48. https://doi.org/10.2151/jmsj.2015-001

Kumar, A., Chen, M., & Wang, W. (2013). Understanding prediction skill of seasonal mean precipitation over the tropics. *Journal of Climate*, 26, 5674–5681. https://doi.org/10.1175/JCLI-D-12-00731.1

Liebmann, B., & Smith, C. A. (1996). Description of a complete (interpolated) outgoing longwave radiation dataset. *Bulletin of the American Meteorological Society*, 77, 1275–1277.

Rayner, N. A., Parker, D. E., Horton, E. B., Folland, C. K., Alexander, L. V., Rowell, D. P., et al. (2003). Global analyses of sea surface temperature, sea ice, and night marine air temperature since the late nineteenth century. *Journal of Geophysical Research*, 108, 4407. https://doi.org/10.1029/2002JD002670

Reynolds, R. W., Smith, T. M., Liu, C., Chelton, C. B., Casey, K. S., & Schlax, M. G. (2007). Daily high-resolution-blended analysis for sea surface temperatures. *Journal of Climate*, 20, 5473–5496. https://doi.org/10.1175/2007JCLI1824.1

Takaya, K., & Nakamura, H. (2001). A formulation of a phase-independent wave-activity flux for stationary and migratory quasigeostrophic eddies on a zonally varying basic flow. *Journal of the Atmospheric Sciences*, 58, 608–627. https://doi.org/10.1175/1520-0469(2001)058<0608:AFOAPI>2.0.CO;2

Takaya, K., & Nakamura, H. (2005). Geographical dependence of upper-level blocking formation associated with intraseasonal amplification of the Siberian High. *Journal of the Atmospheric Sciences*, 62, 4441–4449. https://doi.org/10.1175/JAS3628.1

Tanimoto, Y., Nakamura, H., Kagimoto, T., & Yamane, S. (2003). An active role of extratropical sea surface temperature anomalies in determining anomalous turbulent heat flux. *Journal of Geophysical Research*, 108(C10), 3304. https://doi.org/10.1029/2002JC001750

Trenberth, K. E., & Shea, D. J. (2005). Relationships between precipitation and surface temperature. *Geophysical Research Letters*, 32, L14703. https://doi.org/10.1029/2005GL022760

Wallace, J. M. & Gutzler, D. S. (1981). Teleconnections in the geopotential height field during the Northern Hemisphere winter. *Monthly Weather Review*, 109, 784–812. https://doi.org/10.1175/1520-0493(1981)109%3C0784:TITGHF%3E2.0.CO;2

Wheeler, M. C., & Hendon, H. H. (2004). An all-season real-time multivariate MJO index: Development of an index for monitoring and prediction. *Monthly Weather Review*, 132, 1917–1932. https://doi.org/10.1175/1520-0493(2004)132<1917:AARMMI>2.0.CO;2

Wheeler, M. C., Hendon, H. H., Cleland, S., Meinke, H., & Donald, A. (2009). Impacts of the Madden-Julian Oscillation on Australian rainfall and circulation. *Journal of Climate*, 22, 1482–1498. https://doi.org/10.1175/2008JCLI2595.1

Wu, R., & Kirtman, B. P. (2007). Regimes of seasonal air–sea interaction and implications for performance of forced simulations. *Climate Dynamics*, 29, 393–410. https://doi.org/10.1007/s00382-007-0246-9

Xie, P., & Arkin, P. A. (1997). Global precipitation: A 17-year monthly analysis based on gauge observations, satellite estimates, and numerical model outputs. *Bulletin of the American Meteorological Society*, 78, 2539–2558. https://doi.org/10.1175/1520-0477(1997)078<2539%3AGPAYMA>2.0.CO;2

Xie, S.-P., & Philander, S. G. H. (1994). A coupled ocean-atmosphere model of relevance to the ITCZ in the eastern Pacific. *Tellus*, 46A, 340-350. https://doi.org/10.1034/j.1600-0870.1994.t01-1-00001.x

Supporting Information

Contents of this file

Text S1
Text S2
Figure S1
Figure S2
Figure S3
Figure S4

Introduction

In this supporting information, we describe the separation of anomalous convective activity into SST-forced and SST-unforced components based on observational data. We also describe an atmospheric general circulation mode (AGCM) experiment forced by climatological SST. These results highlight importance of the AUSM variability in tropical convective variability. In addition, we show some supplementary figures.

Text S1.

We have extracted SST-forced and unforced variability of OLR through the following procedure. First, we calculated the five leading empirical orthogonal functions (EOFs) of December-January-February SST over the tropics spanning 20°S–20°N. These five leading modes account for 85% of total SST variance. (We have checked that following results are qualitatively unchanged if we use different number of EOF modes ranging from 3 to 10). Then, we regressed JF OLR anomalies onto each of the corresponding principal component (PC) time series and subtracted them from total OLR anomalies. The residual OLR (rOLR) anomalies are virtually uncorrelated with the tropical SST variability. Thus we refer to the residual as SST-unforced component and sum of the five anomaly fields regressed onto the five leading principal components of tropical SST as SST-forced component of tropical convective variability.

Figures 1d and e show interannual standard deviation of the SST-forced and SST-unforced OLR anomalies, respectively. Because the SST-forced component is mostly explained by El Niño–Southern Oscillation (ENSO), which is extracted as the leading EOF mode of SST and accounts for more than 60% of its total variance, the SST-forced OLR has large standard deviation over the equatorial central Pacific and Maritime Continent (Figure 1d). Interestingly, large variability of the SST-forced component over the Maritime Continent is biased toward the Northern Hemisphere although climatological mean precipitation is shifted toward the Southern Hemisphere. As shown in Figure 1e, southern part of the Maritime Continent and NAUS are the region of largest standard deviation of the SST-unforced component, whose magnitude is comparable to the SST-forced counterpart in the Northern Hemisphere. By comparing Figures 1d and e, we find that most of the anomalous convection over NAUS is not forced by tropical SST anomalies, which is consistent with Figure 2b.

The dominant SST-unforced OLR variability was identified as the leading EOF (EOF1) of rOLR within 30°S–20°N (Figure 1f). EOF1 explains 15% of the rOLR variability. This EOF mode is localized around NAUS, demonstrating a similarity of its pattern to the pattern of precipitation anomaly regressed onto the AUSM index (Figure 2c). The corresponding PC time series is highly correlated with the AUSM index (r = 0.71).

Text S2.

We can extract SST-unforced variability in a relatively simple manner by using an AGCM. We analyze a numerical simulation with the Geophysical Fluid Dynamics Laboratory (GFDL)'s Atmospheric Model version 2.1 (AM2.1, Anderson et al. 2005) to verify our observational results. The model's horizontal resolution is about 220 km, and it consists of 24 vertical levels. We use the result of the climatological ocean (CLIMO) simulation in which SST repeats its climatological seasonal cycle derived from 1982–1998 climatology of NOAA optimum interpolated SST (Reynolds et al. 2007). Grid boxes at which SST is equal to or lower than –1.8ºC are regarded as 100% sea-ice covered. Atmospheric interannual variability in this simulation, which develops in the absence of SST variability, represents the SST-unforced variability. As shown in Figure S1, standard deviation of the JF mean OLR peaks around NAUS. This feature is in common with the result of the decomposition of interannual OLR variability based on the observations shown in Figure 1e.

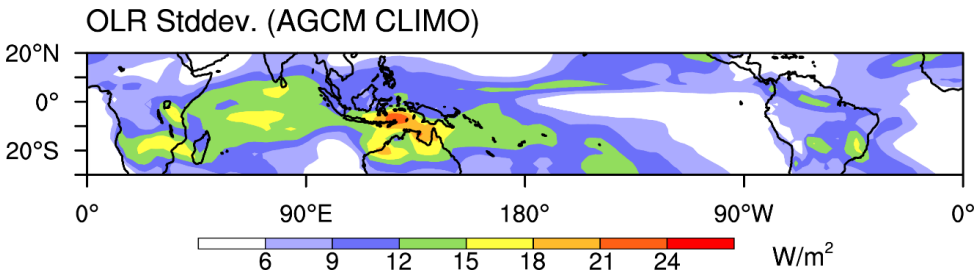

Figure S1. Climatological standard deviation of JF mean OLR in the CLIMO simulation. Details of the numerical experiment are described in Text S2.

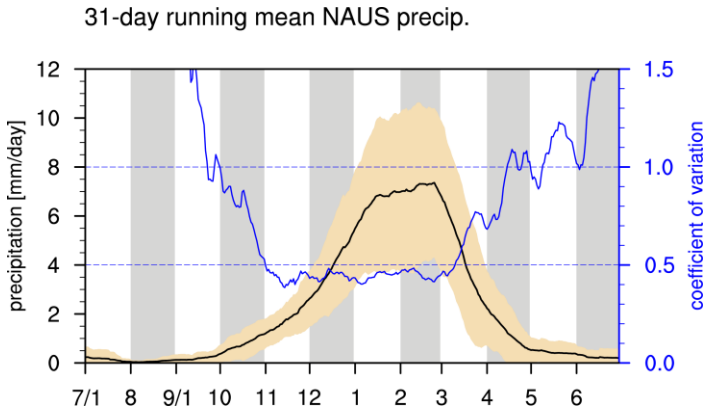

Figure S2. 31-day running mean evolutions of the climatological NAUS precipitation (black line) and the corresponding interannual standard deviation (brown shading). The blue line indicates the coefficient of variation (the ratio of the standard deviation to the climatological mean) of the 31-day running mean precipitation. See also Figure 3a.

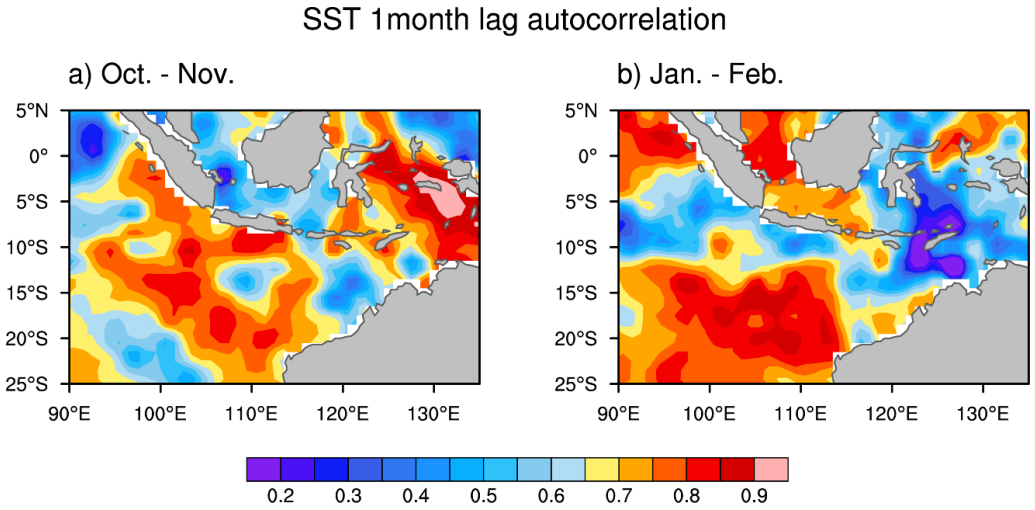

Figure S3. 1-month lag autocorrelation coefficients between (a) October and November, and (b) January and February SST anomalies. (cf. Hendon et al. 2012, their Figure 7)

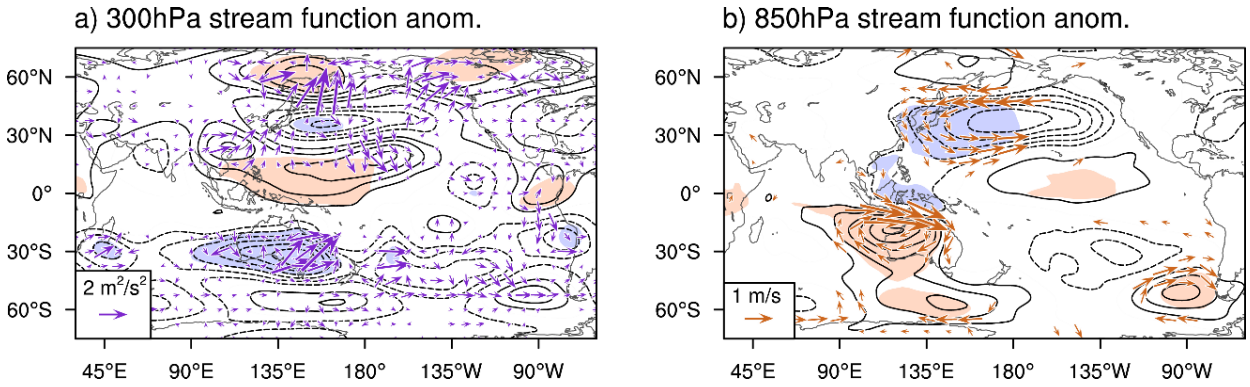

Figure S4. JF streamfunction anomalies at (a) 300 hPa and (b) 850 hPa levels with contour intervals of 5 and 3×10^5 m^2 s^{-1}, respectively. Solid and dashed contours correspond to positive and negative anomalies, respectively, with zero contours omitted. Color shading represents the 95% confidence level. Vectors are (a) Rossby wave-activity flux formulated by Takaya and Nakamura (2001) and (b) 850 hPa wind anomalies, with their scaling given at the left bottom of each panel. Vectors in (b) are plotted only if either of their zonal and meridional components is statistically confident at 95%.